Global Coastal Characteristics (GCC): A global dataset of geophysical, hydrodynamic, and socioeconomic coastal indicators

Panagiotis Athanasiou[1], Ap van Dongeren[1,2], Maarten Pronk[1], Alessio Giardino[3], Michalis Vousdoukas[4], Roshanka Ranasinghe[2, 1, 5]

[1] Deltares, Delft, The Netherlands
[2] Department of Coastal and Urban Risk & Resilience, IHE Delft Institute for Water Education, Delft, The Netherlands
[3] Climate Change and Sustainable Development Department, Asian Development Bank, Manila, Philippines
[4] Department of Marine Sciences, University of the Aegean, Mitilene, Greece
[5] Water Engineering and Management, Faculty of Engineering Technology, University of Twente, Enschede, The Netherlands

Correspondence to: Panagiotis Athanasiou (Panos.Athanasiou@deltares.nl)

Abstract

Around 10 percent of the world's population live in coastal areas that are less than 10 meters above sea level (also known as the low elevation coastal zone – LECZ). Coastal zones are therefore of major importance for local economy, transport and are home to some of the richest ecosystems. This makes coastal zones quite susceptible to extreme storms and sea level rise due to climate change. During the last few years numerous open access global datasets have been published, describing different aspects of the environment such as elevation, land-use, waves, water-levels and exposure. However, for coastal studies it is crucial that this information is available at specific coastal locations and, for regional studies or upscaling purposes, it is also important that data is provided in a spatially consistent manner. Here we create a Global database of Coastal Characteristics (GCC) with 80 indicators covering the geophysical, hydrometeorological and socioeconomic environment, at a high alongshore resolution of 1 km and provided at ~730,000 points along the global ice-free coastline. To achieve this, we use the latest freely available global datasets and a newly created global high-resolution transect system. The geophysical indicators include coastal slopes and elevation maxima, land-use, presence of vegetation or sandy beaches. The hydro-meteorological indicators involve water level, wave conditions and meteorological conditions (rain and temperature). Additionally, socioeconomic indices related to population, GDP and presence of critical infrastructure (roads, railways, ports and airports) are presented. While derived from existing global datasets, these indicators can be valuable for coastal screening studies, especially for data-poor locations.

1   Introduction

Between 750 million and 1.1 billion people live in low-lying coastal areas (MacManus et al., 2021) which is expected to increase in the future (Neumann et al., 2015) . This makes the coast a very important economic area as well as one of the most valuable ecosystems (Paprotny et al., 2021). As a dynamic interface between land and sea, coastal zones are exposed to various

environmental forces (including e.g., waves, currents, and wind) and socio-economic pressures (urbanization, tourism and industry), all of which are continually changing at different spatio-temporal scales. Moreover, sea level rise driven by climate change (IPCC, 2021b) is expected to lead to permanent submergence of low-lying coastal areas, more severe and frequent episodic flooding, shoreline retreat, wetland loss and freshwater degradation due to saltwater intrusion (IPCC, 2021a;

5   Ranasinghe et al., 2021; Glavovic et al., 2022).

The global coastline is quite diverse with various types of landforms including beaches, barrier islands, atolls, river deltas, cliffs, estuaries, and tidal flats, which can respond differently to marine forcing and support different land uses. These different landforms can be usually distinguished by differences in their geophysical and/or hydrometeorological characteristics. The shape of the coast, e.g., slope of the submerged or subaerial profile and average elevation, the presence of vegetation and

10   generally the land cover, are just some of the characteristics that can have a strong influence in the response to increased water levels, flooding, or erosion. On the other hand, offshore marine conditions including wave climate and hydrodynamics are important for the coastal response to marine forcing, while meteorological conditions like temperature and rainfall, can be associated with local vegetation and geology. Additionally, information on the local presence of population, assets and infrastructure is critical for coastal impact and risk assessments and identifying vulnerable areas.

15   Due to the ever-increasing Earth observations and computational power, large-scale coastal impact assessments have become more frequent in literature during the past years. One of the first attempts of a coastal vulnerability assessment at the global scale, was the DIVA tool (Vafeidis et al., 2008; Hinkel and Klein, 2009), which although state-of-the-art at the time of its development, used predefined segments at a relatively coarse resolution (Wolff et al., 2016; Athanasiou, 2022), and was based on lower resolution and accuracy datasets, available at the time. Satellite imagery has been used at the global scale as well, to

20   get insights of the global dynamics of shoreline change at sandy beaches (Luijendijk et al., 2018); global land erosion/accretion trends (Mentaschi et al., 2018); shoreline change due to El Niño along Pacific coastlines (Vos et al., 2023) and at the global scale (Almar et al., 2023); identifying coastal vegetation (van Zelst et al., 2021); or deriving beach face slopes for Australia (Vos et al., 2022). Moreover, in Young et al. (2019), the global distribution of coastal cliffs was assessed using the SRTMv3 global digital elevation model (DEM). Athanasiou et al. (2019), used a combination of the global DEM MERIT and the

25   bathymetric map of GEBCO, to estimate nearshore slopes, while in Vousdoukas et al. (2020b), future shoreline change was assessed at sandy beaches globally. In Almar et al. (2021), coastal overtopping was assessed globally, using slope and coastal maximum data derived from the global DEM ALOS, but using a relative course grid along the global coastline. Additionally, large scale coastal flooding has been assessed at the European (Vousdoukas et al., 2018, 2020a) and the global scale (Kirezci et al., 2020; Tiggeloven et al., 2020) using extreme water level boundary conditions and global DEMs.

30   During the last few years, new open access global datasets are becoming available. The latest freely available global DEM with a high resolution of 1 arcsecond (~ 30 m at the equator) is the CopernicusDEM (Airbus Defence and Space GmbH, 2020). However, this type of DEM captures the surface rather than the terrain elevation, making them inaccurate in vegetated and

urban environments. In an attempt to correct for these effects, new DEMs have been produced correcting the elevations in vegetated and urbanized areas, such as FABDEM (Hawker et al., 2022), which is however not in the public domain, and more recently the open access DeltaDEM (Pronk, 2023). Moreover,,the European Space Agency (ESA) produced a new land-cover dataset at a high resolution of 10 m (Zanaga et al., 2021), while continuously updated global reanalysis products like ERA5

5   (Hersbach et al., 2020) provide an unprecedent representation of the historical climate conditions globally, and global hydrodynamic modelling (Muis et al., 2020) provide information on global water levels statistics. Additionally, global population maps with a high resolution of 100 m from WorldPop (Bondarenko et al., 2020), and global mapping of infrastructure using crowd sourcing techniques (OpenStreetMap contributors, 2017), provides an enormous wealth of information on the exposed population and assets.

10   In this work, we use all these recent developments in global data to extract a large set of indicators at the coast. We present a compiled global database of coastal characteristics (Global Coastal Characteristics – GCC) based on indicators of the geophysical, hydrometeorological and socioeconomic environment (Figure 1). The geophysical indicators are related to the profile shape characteristics (e.g., slope, elevation maxima et al.), presence of sandy beach or vegetation and land cover (e.g., build-up areas, forest etc.). The hydrodynamic indicators include offshore water level and wave conditions, and meteorological

15   conditions (rain and temperature). Furthermore, socioeconomic indicators related to population, GDP and presence of critical infrastructure (roads, railways, ports and airports) are also included. For the extraction of all these different types of indicators, we use available open access global datasets and generated a global transect system at a 1 km interval, resulting in ~730,000 points along the global ice-free coastline. To our knowledge, this is the first time that such a high number of diverse indicators, covering the spectrum between the geophysical characteristics, offshore marine environment, and socioeconomic conditions,

20   are brought together on a common high-resolution grid, using state-of-the-art open access datasets. While based on global data, we believe that this dataset can be valuable for initial case study descriptions in data poor environments, quick coastal screening studies or for broad coastal classification purposes. However, it should be noted that, given the resolution of the parent data sets and underlying assumptions, the database presented here should not be used for detailed local scale modelling or assessments.

25   The paper is structured as follows: the underlying data and methodologies used to derive the indicators are described in Section 2. The results, including the definitions of all extracted indicators, and a set of global statistics and maps are presented in Section 3. The paper concludes with a discussion on the limitations associated with the presented dataset and an overview of its potential applications, with an example of a global classification of coasts using unsupervised machine learning.

2   Materials and methods

The prerequisites for all data sets used here to extract coastal indicators was that the datasets were recent open-access and had a global coverage. An overview of the data sets used is given in Table 1. The generation of a global transect system and the methods to extract the various indicators from the datasets, based on these transects, are presented in the next sections.

2.1   Transect system

A global transect system was generated using an along-coast spacing of 1 km in the zoom level 8 generalized version of the Open Street Maps (OSM) coastline vector (Generalized coastlines, 2016) , which is a simplified version that removes fine details of the coastline (e.g., rocky outcrops) and has been previously used for other global transect systems (Luijendijk et al., 2018; Athanasiou et al., 2019). First, a simple smoothing procedure was applied on the coastline to ensure that there were no sharp corners that could lead to misalignments of the transects. Since our analysis focused on the ice-free coastal areas, coastlines in the South Pole (Antarctica) and at the North Pole (Greenland, and parts of Canada and Russia) were excluded from the analysis following Luijendijk et al. (2018). This resulted in 728,088 cross-shore transects globally (Figure 2). The transects extended 4 km in both the landward and seaward directions from their centroid, which was defined at the OSM location (which, since we use a generalized coastline, is not necessarily the shoreline location). A total profile length of 8 km was chosen after testing different lengths to ensure a good coverage of the coastal zone, while avoiding unnecessarily high data-storage (Athanasiou et al., 2019). The longitude and latitude of each centroid was extracted for each transect along with the transect orientation.

2.2   Raster data extraction

Various raster-based datasets were used to extract elevation, land cover and population information at each transect. This was performed with one of the following approaches, as appropriate: 1) by extracting a cross-shore profile of values along each transect or 2) by performing zonal statistics in a buffer area around the landward part of each transect (Figure 3).

Profiles were extracted from the topography, bathymetry, land-mask, land cover and water occurrence rasters (Table 1). Along each transect, two 1D grids with different cross-shore resolutions were defined; a coarse grid with a spacing of 25 m and a finer grid with a spacing of 10 m. This was done to ensure that raster datasets with different resolutions will be captured in detail, while also reducing the data-storage. The profiles of topography (both for CopernicusDEM and DeltaDEM) and bathymetry (GEBCO) were extracted along the coarse 25 m grid. The land mask (CopernicusDEM) and water occurrence (JRC) profiles were extracted on the same coarse grid. Finally, the land cover (ESA WorldCover) profile was extracted on the finer 10 m grid.

Zonal statistics were performed on the land cover (ESA WorldCover) and population (WorldPop) rasters using buffer zones of 500 m width around the transects (Figure 3). It should be noted that these buffer zones can be overlapping or not cover the

whole 4 km (sub-aerial) zone, depending on the orientation of the coastline (see Section 4 for more details). For the land cover, the occurrence of each land cover class in the buffer zone was calculated for each transect. For the population, the total population in the buffer zone was calculated per transect and in addition, the number of people located below specific elevation thresholds (1, 5 and 10 m above MSL) was estimated using the topography raster. To achieve this, the elevation raster was re-sampled to the population raster grid using averaging, and then masks were created when the elevation cells were below the respective elevation thresholds.

2.3 Vector data extraction

Various GIS methods were used to extract data from other datasets (Table 1) that were in points or lines (vector) format (Figure 4).

To assess whether a transect is sandy or not, the sandy locations from Luijendijk et al. (2018) were used. In that study, a different transect system (with 500 m alongshore spacing) was employed to classify coastal locations as sandy or not, using machine learning methods on satellite imagery. To classify our transects as sandy or not, proximity analysis was used (see Figure 4a) to determine the presence of sandy points from Luijendijk et al. (2018) in a 1 km buffer zone around the centroid of our transects. We followed the same approach to assess whether there is coastal vegetation that can protect the coast (i.e. mangroves or salt marshes) at a transect by using the data points from van Zelst et al. (2021). A 1 km proximity analysis was also used to assess whether there are ports (using the World Port Index) or airports (using the Global Airport Database) in the vicinity of the transects.

To assess whether there are roads or railways at the transects, we performed an intersection analysis (see Figure 4b), where we determined whether a transect is intersecting with any line that represents a road (using the gRoads_v1 dataset) or a railway (using the Global Railways dataset).

Finally, to sample indicators describing continuous variables from point vector datasets, we used an inverse distance interpolation using the two closest points to each transect (see Figure 4c). These indicators were associated with wave and meteorological data from ERA5, water level data from GTSM_v3.0 and gridded GDP data from Kummu et al. (2018). Only the two closest points that were in a zone of 100 km around each transect were used in the process, to avoid sampling of points that were far away and thus not descriptive of the transect's conditions. Since the gridded data in Kummu et al. (2018) do not offer a full coverage globally (e.g., Pacific SIDS), we additionally extracted GDP/capita using a country identifier for each transect and the country GDP/capita information from the World Bank (2022).

The ERA5 wave data are available only at offshore locations due the coarse spatial resolution of the wave grid (~30 km). These conditions are not descriptive of the local wave environment at each transect. However, transforming 30 years of wave time-series to ~1 million locations globally was out of the scope of the present study. To this end, all the wave indicators at each transect were sampled from the two closest ERA5 offshore points, with a 100 km maximum distance. The same approach was

followed for the water level indicators that were extracted from GTSM_v3.0, from which we sampled indicators related to the tidal level (TL), storm surge level (SSL) and the total water level (TWL, including the mean sea level, tide and storm surge).

2.4   Profile indicators extraction

To create a continuous elevation profile including both the submerged and subaerial parts of the coastal profile, the topographic

5   and bathymetric profiles were merged. Two elevation profiles were created per transect, one using the CopernicusDEM and one using the DeltaDEM as the topography source. The following steps were followed : 1) The CopernicusDEM mask profile was used to define the land cells, 2) The CopernicusDEM/DeltaDEM topography profile values were used for the land cell elevations after they were transformed from "m above geoid" to "m above MSL" using the mean dynamic topography map (DTU10_MDT), 3) Then the finer resolution "open water" class for the ESA World Cover raster was used to define the sea

10   cells, 4) For the sea cells, the bathymetric raster values were used only when they were below MSL. If there were points that ESA World Cover was showing as land but the CopernicusDEM mask was indicating as water, an elevation of 0.2 m was used. Similarly, at the locations where the ESA World Cover was showing as water but GEBCO was showing as land, an elevation of -0.2 m was used. This was performed to ensure that at least the cross-shore location of the shoreline was based on the finer resolution of the ESA World Cover.

15   For each of the merged elevation profiles a set of locations that define specific areas of the profile were identified (Figure 5). The Depth of Closure (DoC) describes the depth seaward of which there is no significant change in bottom elevation and is determined by the wave statistics (Hallermeier, 1978). In Athanasiou et al. (2019), an offshore wave reanalysis was used to estimate the DoC along the global coastline, with a temporal scale of 34 years following Nicholls et al. (1998). Here, the DoC at each transect was estimated by applying an inverse distance interpolation using the DoC values of the two closest offshore

20   points from Athanasiou et al. (2019). A limit of 150 km was used, to avoid transects getting values that are non-representative of their offshore wave environments. While the depth of closure is a concept only valid for sandy coasts, here it is used broadly for all types of coasts to have an offshore limit for the profile shape calculations. In case there was no offshore point for DoC in the proximity, a default value of 10 m was used, and a warning was transcribed. The actual location of the DoC was calculated with respect to the Mean Lower Low Water (MLLW), as extracted at the transect location from GTSM_v3.0 (see

25   previous section). In case the subaqueous profile had more than one intersection with the DoC elevation, the most landward location was selected.

The location of the shoreline was identified as the most seaward location where the elevation profile crossed the value of 0 m, in a 1 km window around the centroid of the transect (which is the location of the smoothed OSM coastline). Then two different coastal maxima were identified landwards of the shoreline using two different methods. The coastal max (first peak) was

30   identified by finding the first elevation peak landwards of the shoreline (Almar et al., 2021). The coastal max (max peak 1km) was identified by finding the maximum elevation peak in a 1 km window landwards of the shoreline. These two coastal maxima can act as a proxy of the local flood protection level. For both coastal maxima location, the land cover type was extracted as

well. The area landwards of the coastal max (first peak) was defined as the hinterland, for which the average hinterland elevation (he) and elevation variance (ev) were extracted.

The area between the depth of closure and the shoreline was defined as the nearshore (Athanasiou et al., 2019) and the nearshore slope (ns) was calculated as:

$$ns = \frac{z_{shoreline} - z_{DoC}}{x_{shoreline} - x_{DoC}} \tag{1}$$

5   The area between the shoreline and the coastal max (first peak) was defined as the backshore area and the backshore slope (bs) was calculated as:

$$bs = \frac{z_{coastal\_max\_first\_peak} - z_{shoreline}}{x_{coastal\_max\_first\_peak} - x_{shoreline}} \tag{2}$$

The coastal slope (cs) was calculated as well, defined as the slope between the depth of closure and the Coastal max (first peak). The coastal slope was calculated as:

$$cs = \frac{z_{coastal\_max\_first\_peak} - z_{DoC}}{x_{coastal\_max\_first\_peak} - x_{DoC}} \tag{3}$$

All the previously described indicators that included an elevation maxima in their calculation, were extracted twice for
10   elevation profiles derived from both the CopernicusDEM and DeltaDEM to ensure that in case of potential overcorrections of the DeltaDEM the CopernicusDEM derived values are available (see Table 2 and Section 4.1).

Finally, the width of the transition zone was extracted as cross-shore distance between the points around the shoreline with a 5 and 95 % water occurrence as indicated in the JRC water occurrence map. This indicator combines information on the local tidal range and slope of the intertidal zone, but care should be taken with its interpretation since it could be affected by natural
15   morphodynamics or human-induced changes.

3   Results

3.1   Geophysical indicators

A list of all the geophysical indicators extracted along with a description of each indicator and its label used in the GCC database is given in Table 2. As explained in the previous section the indicators that involved estimation of elevation maxima
20   were extracted for both CopernicusDEM (copdem) and DeltaDEM (deltadem). As an example, a global map of the coastal max (max peak 1 km) using deltadem is presented in Figure 6, along with some global statistics. A median coastal max of 13.64 m above MSL is found globally, with quite distinct spatial differences globally relating to the shape of the coast. The

mode of the coastal max globally is between 3 and 4 m, while the 5th and 95th percentiles are 0.9 m and 260 m respectively. The peak in the distribution just above 100 m can be explained by the correction algorithm of DeltaDEM, which is limited above 100 m. For 12.11 % of the global transects, a coastal max with this method could not be calculated, since there was no elevation peak in the 1 km zone.

3.2 Hydrodynamic indicators

A list of all the hydrodynamic indicators extracted along with a description of each indicator and its label used in the GCC database is given in Table 3. As an example, a global map of the Average MWD of Hs ≥ Hs_p95 is presented in Figure 7, along with some global statistics. A median H_s (95th percentile) of 210 deg is found globally, with quite distinct spatial differences globally relating to global wind-patterns and the orientation of the coastline.

3.3 Socioeconomic indicators

A list of all the socio-economic indicators extracted along with a description of each indicator and its label used in the GCC database is given in Table 4. As an example, a global map of the population at elevation < 10 m is presented in Figure 8, along with some global statistics. More than 50% of the transects have 0 population at elevation < 10 m, while for the transects that have at least 1 person, the median value is ~200 people, with a distribution that is close to a normal distribution in the logarithmic scale. The 25th and 75th percentile values are 40 and 1000 people respectively.

4 Discussion

4.1 Limitations

Bringing together a wide range of different datasets, describing geophysical, hydrometeorological, ecological and socio-economic characteristics, under a common, relatively high-resolution spatial grid provides an unprecedented holistic view of the global coastline. Nevertheless, while global datasets provide an (almost) global coverage, they arguably suffer from numerous shortcomings related to accuracy and resolution. Therefore, the developed indicators of the GCC dataset should not be seen as a replacement for local-scale studies or data-collection and monitoring campaigns and should not be directly employed for very local scale efforts such as, for e.g., designing coastal adaptation measures or informing decision making. On the other hand, the dataset presented herein can be a valuable tool for getting initial insights at data-poor environments; coastal screening studies for identifying hazard/impact hotspots where more detailed assessment should take place (van Dongeren et al., 2018); or coastal assessments at regional, continental or global scales, where aggregated statistics are suitable. Since all our indicators are based on open access datasets, the methodologies used for their generation, detailed information on their accuracy, and underlying assumptions can be found in their respective references (Table 1). Therefore, here we only briefly discuss the main limitations in the original datasets or those introduced in our data processing to derive the indicators.

When combining topographic and bathymetric elevation data from different sources and with different resolutions, the transition zone between sea and land can be a challenging area to correctly resolve. Here, since we focused on the derivation of indicator, as opposed to reproducing accurate depths and elevations in this transition area, we employed the land-use map to distinguish between land and sea (see Section 2.4). In this way we have more confidence in the cross-shore location of the shoreline, which is used for the extraction of different slope indicators. An improvement would be to explore how EO derived intertidal bathymetry could be used to obtain better estimates in this transition zone (Mason et al., 1995).

Moreover, as mentioned in the introduction, global DEMs like CopernicusDEM, suffer from biases in areas with high vegetation and buildings. Corrected DEMs, like FABDEM and DeltaDEM account for these biases and produce elevation maps far closer to the actual terrain elevation. However, it has been observed, that due to the underlying algorithms applied for this correction, they can in some cases overcorrect narrow features like dunes and dikes, reducing their elevations. For this type of locations, CopernicusDEM was found to perform better in capturing the elevation (when compared with local in-situ data). Thus, in the GCC dataset we have provided all the elevation related parameters, both for CopernicusDEM and DeltaDEM. In areas with narrow, vegetation-less dunes, CopernicusDEM will capture coastal maxima more accurately, while in areas with coastal vegetation, DeltaDEM will produce better results. For indicators such as the mean hinterland elevation and population below given elevations, which cover larger areas rather than narrow features, DeltaDEM derived indicators are likely to be more accurate, that is why we provide a single value.

The population and land-use indicators that were extracted from the buffer zones around the transects (see Figure 3), give an indication of the local transect conditions, but do not necessarily depict spatially representative values. For example, when the coast has a convex shape (e.g., at a peninsula) the transects and thus buffer zones can overlap, meaning that the same cell of population or land-use from the initial raster datasets can be counted in more than one transect. On the other hand, when the coast has a concave shape (e.g., at an embayment), the buffer zones will not cover the entire area 4 km landwards of the shoreline, as the transects will diverge over land. Furthermore, at narrow islands too the transects and their buffer zones may overlap (see Figure 2).

Another limitation of the GCC dataset is with respect to the wave related indicators, which are sampled at the local transect level from ERA5 offshore points around a 100 km buffer zone with a simple inverse distance interpolation. An offshore to nearshore wave transformation for almost one million locations globally is beyond the scope of this global dataset. However, this methodological constraint can lead to significant differences between the wave indicators extracted and the actual wave conditions at each transect, where the resolution of the ERA5 wave grid cannot represent the shape of the coastline and wave refraction/diffraction effects on nearshore wave conditions.

It is important to note that our indicators in the GCC dataset set presents a static image of the coast. However, a large part of the global coastline can be quite dynamic in response to hydrometeorological forcing and/or human developments. Using global-DEMs allows us to capture a moment in time of the shape of the coastline, which will produce inconsistencies in highly

dynamic areas or fast developing areas. The same holds for the land-use data, which can have seasonal variations and more permanent changes especially in highly developed coastal zones. Latest developments using satellite imagery to produce near real time land-use maps (Brown et al., 2022) indicate that the dynamic component of land-use could potentially be taken into account, while in the future similar techniques could allow for better representation of dynamic elevations when the respective

5 sensors and techniques develop further. Except from the data that are used to sample the indicators at the transect level, this dynamic component of the coast can affect the location and number of transects themselves, while in some cases inconsistencies between the timing of the shoreline and DEM data can result in non-representative indicators.

4.2 Potential applications

The GCC dataset can have numerous applications. For example, coastal screening tools using indices; like the coastal

10 vulnerability index (CVI) have been commonly applied at large spatial scales for impact assessments (Rocha et al., 2023; Pantusa et al., 2022). These tools depend on various indices related to the geophysical shape, hydrodynamic forcing and exposure; and the indicators produced herein could directly be used for this purpose. Furthermore, these indicators could be useful for gaining initial insights for high-level studies aimed at planning future regional or country scale developments.

During the past years various studies have assessed climate change impacts on coasts globally including sandy beach erosion

15 (Athanasiou et al., 2019, 2020; Vousdoukas et al., 2020b) and coastal flooding (Kirezci et al., 2020; Tiggeloven et al., 2020; Almar et al., 2021; van Zelst et al., 2021). For this type of studies the produced indicators in GCC can be a valuable input in combinations with climate-change scenarios (IPCC, 2021b), enabling the assessment of future coastal impacts in a globally consistent way. For example, the nearshore slope can be used for assessing wave transformation and sea level rise induced shoreline retreat, while the backshore slope can be employed for estimating wave run-up. Also, the coastal maxima and

20 hinterland elevation indicators may be used as a representation of the coastal protection level, potentially replacing purely qualitative rules-based approaches (Scussolini et al., 2016).

The typology of the coast can dictate its vulnerability to environmental forcing and future climate change. For large scale assessments this classification is valuable to differentiate between different hazards and the relevant approaches that are needed to assess the impacts at different parts of the coast. Coastal classification relies on coastal indicators in order to group coastlines

25 of a certain type together (Finkl, 2004; Rosendahl Appelquist and Halsnæs, 2015; Dang et al., 2020; Mao et al., 2022). As a showcase of the potential use of the dataset presented here for coastal classification, we demonstrate the application of an unsupervised global classification based on a set of geophysical indicators, grouping the global coastline based on its geophysical shape. For this, we apply a K-Means clustering, following the approach in Athanasiou et al. (2021), using six geophysical indicators from the presented GCC database: 1) Coastal Max (max peak 1 km) , 2) Mean hinterland elevation , 3)

30 Nearshore slope, 4) Backshore slope, 5) Open-water land cover class occurrence, and 6) Transition zone width. Since this is not a dedicated global coastal classification analysis, but rather an indicative application of the presented dataset, we only use 9 clusters (Figure 9). This value can be quite low for a global clustering, but it allows for easy visualization of the results. Due

to the choice of the low number of clusters, the intra-cluster variability of the elevation profiles is quite high (Figure 9c). This high variability can be identified by the large envelopes of the 5th-95th percentile range in the cross-shore elevation profiles for each cluster. However, there are distinct shapes between the different clusters. For example, clusters 3 and 7 represent coastlines with high coastal maxima, high hinterland elevation and steep slopes, which, as seen in the global map in Figure 9a can be connected with fjord areas (e.g. Norway and Chile). On the other hand, cluster 6 shows the highest occurrence of open-water landwards of the shoreline and generally low elevations, which can be connected with atoll islands (e.g. Pacific SIDS).

5   Data Availability

The GCC dataset can be accessed at Zenodo under https://doi.org/10.5281/zenodo.8200200 (Athanasiou, 2023). The dataset is composed of three comma separated values (.csv) files with the global geophysical, hydrodynamic and socioeconomic indicators respectively and a metadata file describing all the indicators included in the csv files.

6   Conclusions

Here, we provide a 1 km along-coast resolution dataset of 80 coastal indicators describing the geophysical, hydrometeorogical, and socio-economic conditions along the global ice-free coastline. This dataset offers a collection of indicators that can be useful for coastal screening studies, quick overviews of coastal environment anywhere in the world, and for coastal classification. The indicators were extracted based on various open-source global datasets that were available at the time of undertaking this work, but can be updated using the same workflow, whenever new datasets become available.

Author contribution

PA, AvD, AG, MV, and RR designed the study. PA carried out the data processing and analysis. MP created the corrected DEM used in the study and assisted with the DEM related parts. PA prepared the paper with contributions from all co-authors.

Competing interests

The authors declare that they have no conflict of interest.

Disclaimer

The views expressed in the article do not reflect the views of ADB.

Acknowledgements

RR is partly supported by the AXA Research Fund. PA and AvD were partly funded through a contract with the Joint Research Centre of the European Commission.

References

Airbus Defence and Space GmbH: Copernicus DEM Product Handbook, 2020.

Almar, R., Ranasinghe, R., Bergsma, E. W. J., Diaz, H., Melet, A., Papa, F., Vousdoukas, M., Athanasiou, P., Dada, O., Almeida, L. P., and Kestenare, E.: A global analysis of extreme coastal water levels with implications for potential coastal overtopping, Nat. Commun., 12, 3775, https://doi.org/10.1038/s41467-021-24008-9, 2021.

Almar, R., Boucharel, J., Graffin, M., Abessolo, G. O., Thoumyre, G., Papa, F., Ranasinghe, R., Montano, J., Bergsma, E. W. J., Baba, M. W., and Jin, F.-F.: Influence of El Niño on the variability of global shoreline position, Nat. Commun., 14, 3133, https://doi.org/10.1038/s41467-023-38742-9, 2023.

Athanasiou, P.: Assessing coastal erosion hazards at large spatial scales: Insights and uncertainties, https://doi.org/10.3990/1.9789036554282, 2022.

Athanasiou, P.: Global Coastal Characteristics (GCC): A global dataset of geophysical, hydrodynamic, and socioeconomic coastal indicators (v1.0), https://doi.org/10.5281/zenodo.8200200, 2023.

Athanasiou, P., van Dongeren, A., Giardino, A., Vousdoukas, M., Gaytan-Aguilar, S., and Ranasinghe, R.: Global distribution of nearshore slopes with implications for coastal retreat, 15, 2019.

Athanasiou, P., van Dongeren, A., Giardino, A., Vousdoukas, M. I., Ranasinghe, R., and Kwadijk, J.: Uncertainties in projections of sandy beach erosion due to sea level rise: an analysis at the European scale, Sci. Rep., 10, 11895, https://doi.org/10.1038/s41598-020-68576-0, 2020.

Athanasiou, P., van Dongeren, A., Giardino, A., Vousdoukas, M., Antolinez, J. A. A., and Ranasinghe, R.: A Clustering Approach for Predicting Dune Morphodynamic Response to Storms Using Typological Coastal Profiles: A Case Study at the Dutch Coast, Front. Mar. Sci., 8, 747754, https://doi.org/10.3389/fmars.2021.747754, 2021.

Bondarenko, M., Kerr, D., Sorichetta, A., and Tatem, A.: Census/projection-disaggregated gridded population datasets, adjusted to match the corresponding UNPD 2020 estimates, for 183 countries in 2020 using Built-Settlement Growth Model (BSGM) outputs, https://doi.org/10.5258/SOTON/WP00685, 2020.

Brown, C. F., Brumby, S. P., Guzder-Williams, B., Birch, T., Hyde, S. B., Mazzariello, J., Czerwinski, W., Pasquarella, V. J., Haertel, R., Ilyushchenko, S., Schwehr, K., Weisse, M., Stolle, F., Hanson, C., Guinan, O., Moore, R., and Tait, A. M.: Dynamic World, Near real-time global 10 m land use land cover mapping, Sci. Data, 9, 251, https://doi.org/10.1038/s41597-022-01307-4, 2022.

Dang, K. B., Dang, V. B., Bui, Q. T., Nguyen, V. V., Pham, T. P. N., and Ngo, V. L.: A Convolutional Neural Network for Coastal Classification Based on ALOS and NOAA Satellite Data, IEEE Access, 8, 11824–11839, https://doi.org/10.1109/ACCESS.2020.2965231, 2020.

van Dongeren, A., Ciavola, P., Martinez, G., Viavattene, C., Bogaard, T., Ferreira, O., Higgins, R., and McCall, R.: Introduction to RISC-KIT: Resilience-increasing strategies for coasts, Coast. Eng., 134, 2–9, https://doi.org/10.1016/j.coastaleng.2017.10.007, 2018.

Finkl, C. W.: Coastal Classification: Systematic Approaches to Consider in the Development of a Comprehensive Scheme, J. Coast. Res., 201, 166–213, https://doi.org/10.2112/1551-5036(2004)20[166:CCSATC]2.0.CO;2, 2004.

GEBCO Bathymetric Compilation Group: The GEBCO_2023 Grid - a continuous terrain model of the global oceans and land. (1), https://doi.org/10.5285/F98B053B-0CBC-6C23-E053-6C86ABC0AF7B, 2023.

Glavovic, B. C., Dawson, R., Chow, W., Garschagen, M., Haasnoot, M., Singh, C., and Thomas, A.: Cross-Chapter Paper 2: Cities and Settlements by the Sea, edited by: Pörtner, H. O., Roberts, D. C., Tignor, M., Poloczanska, E. S., Mintenbeck, K.,
5 Alegría, A., Craig, M., Langsdorf, S., Löschke, S., Möller, V., Okem, A., and Rama, B., Clim. Change 2022 Impacts Adapt. Vulnerability Contrib. Work. Group II Sixth Assess. Rep. Intergov. Panel Clim. Change, 2163–2194, https://doi.org/10.1017/9781009325844.019.2163, 2022.

Hallermeier, R. J.: Uses for a calculated limit depth to beach erosion, Coast. Eng., 20, 1978.

Hawker, L., Uhe, P., Paulo, L., Sosa, J., Savage, J., Sampson, C., and Neal, J.: A 30 m global map of elevation with forests
10 and buildings removed, Environ. Res. Lett., 17, 024016, https://doi.org/10.1088/1748-9326/ac4d4f, 2022.

Hersbach, H., Bell, B., Berrisford, P., Hirahara, S., Horányi, A., Muñoz-Sabater, J., Nicolas, J., Peubey, C., Radu, R., Schepers, D., Simmons, A., Soci, C., Abdalla, S., Abellan, X., Balsamo, G., Bechtold, P., Biavati, G., Bidlot, J., Bonavita, M., Chiara, G., Dahlgren, P., Dee, D., Diamantakis, M., Dragani, R., Flemming, J., Forbes, R., Fuentes, M., Geer, A., Haimberger, L., Healy, S., Hogan, R. J., Hólm, E., Janisková, M., Keeley, S., Laloyaux, P., Lopez, P., Lupu, C., Radnoti, G., Rosnay, P.,
15 Rozum, I., Vamborg, F., Villaume, S., and Thépaut, J.: The ERA5 global reanalysis, Q. J. R. Meteorol. Soc., 146, 1999–2049, https://doi.org/10.1002/qj.3803, 2020.

Hinkel, J. and Klein, R. J. T.: Integrating knowledge to assess coastal vulnerability to sea-level rise: The development of the DIVA tool, Glob. Environ. Change, 19, 384–395, https://doi.org/10.1016/j.gloenvcha.2009.03.002, 2009.

IPCC: Summary for Policymakers, edited by: Masson-Delmotte, V., Zhai, P., Pirani, A., Connors, S. L., Péan, C., Berger, S.,
20 Caud, N., Chen, Y., Goldfarb, L., Gomis, M. I., Huang, M., Leitzell, K., Lonnoy, E., Matthews, J. B. R., Maycock, T. K., Waterfield, T., Yelekçi, O., Yu, R., and Zhou, B., Clim. Change 2021 Phys. Sci. Basis Contrib. Work. Group Sixth Assess. Rep. Intergov. Panel Clim. Change, 3−32, https://doi.org/10.1017/9781009157896.001, 2021a.

IPCC: Summary for Policymakers. In: Climate Change 2021: The Physical Science Basis. Contribution of Working Group I to the Sixth Assessment Report of the Intergovernmental Panel on Climate Change [Masson-Delmotte, V., P. Zhai, A. Pirani,
25 S.L. Connors, C. Péan, S. Berger, N. Caud, Y. Chen, L. Goldfarb, M.I. Gomis, M. Huang, K. Leitzell, E. Lonnoy, J.B.R. Matthews, T.K. Maycock, T. Waterfield, O. Yelekçi, R. Yu, and B. Zhou (eds.)], Cambridge University Press, Cambridge, United Kingdom and New York, NY, USA, https://doi.org/10.1017/9781009157896.001., 2021b.

Kirezci, E., Young, I. R., Ranasinghe, R., Muis, S., Nicholls, R. J., Lincke, D., and Hinkel, J.: Projections of global-scale extreme sea levels and resulting episodic coastal flooding over the 21st Century, Sci. Rep., 10, 11629,
30 https://doi.org/10.1038/s41598-020-67736-6, 2020.

Knudsen, P. and Andersen, O. B.: A GLOBAL MEAN OCEAN CIRCULATION ESTIMATION USING GOCE GRAVITY MODELS – THE DTU12MDT MEAN DYNAMIC TOPOGRAPHY MODEL, 6, 2013.

Kummu, M., Taka, M., and Guillaume, J. H. A.: Gridded global datasets for Gross Domestic Product and Human Development Index over 1990–2015, Sci. Data, 5, 180004, https://doi.org/10.1038/sdata.2018.4, 2018.

35 Luijendijk, A., Hagenaars, G., Ranasinghe, R., Baart, F., Donchyts, G., and Aarninkhof, S.: The State of the World's Beaches, Sci. Rep., 8, 6641, https://doi.org/10.1038/s41598-018-24630-6, 2018.

MacManus, K., Balk, D., Engin, H., McGranahan, G., and Inman, R.: Estimating population and urban areas at risk of coastal hazards, 1990–2015: how data choices matter, Earth Syst. Sci. Data, 13, 5747–5801, https://doi.org/10.5194/essd-13-5747-2021, 2021.

5 Mao, Y., Harris, D. L., Xie, Z., and Phinn, S.: Global coastal geomorphology – integrating earth observation and geospatial data, Remote Sens. Environ., 278, 113082, https://doi.org/10.1016/j.rse.2022.113082, 2022.

Mason, D. C., Davenport, I. J., Robinson, G. J., Flather, R. A., and McCartney, B. S.: Construction of an inter-tidal digital elevation model by the 'Water-Line' Method, Geophys. Res. Lett., 22, 3187–3190, https://doi.org/10.1029/95GL03168, 1995.

Meijer, J. R., Huijbregts, M. A. J., Schotten, K. C. G. J., and Schipper, A. M.: Global patterns of current and future road infrastructure, Environ. Res. Lett., 13, 064006, https://doi.org/10.1088/1748-9326/aabd42, 2018.

10 Mentaschi, L., Vousdoukas, M. I., Pekel, J.-F., Voukouvalas, E., and Feyen, L.: Global long-term observations of coastal erosion and accretion, Sci. Rep., 8, 12876, https://doi.org/10.1038/s41598-018-30904-w, 2018.

Muis, S., Apecechea, M. I., Dullaart, J., de Lima Rego, J., Madsen, K. S., Su, J., Yan, K., and Verlaan, M.: A High-Resolution Global Dataset of Extreme Sea Levels, Tides, and Storm Surges, Including Future Projections, Front. Mar. Sci., 7, 263, https://doi.org/10.3389/fmars.2020.00263, 2020.

15 National Geospatial-Intelligence Agency: World Port Index, Springfield, VA, USA, 2019.

Neumann, B., Vafeidis, A. T., Zimmermann, J., and Nicholls, R. J.: Future Coastal Population Growth and Exposure to Sea-Level Rise and Coastal Flooding - A Global Assessment, PLOS ONE, 10, e0118571, https://doi.org/10.1371/journal.pone.0118571, 2015.

Nicholls, R. J., Birkemeier, W. A., and Lee, G.: Evaluation of depth of closure using data from Duck, NC, USA, Mar. Geol.,
20 148, 179–201, https://doi.org/10.1016/S0025-3227(98)00011-5, 1998.

Generalized coastlines: https://osmdata.openstreetmap.de/data/generalized-coastlines.html, last access: 10 November 2016.

OpenStreetMap contributors: Planet dump retrieved from https://planet.osm.org, 2017.

Pantusa, D., D'Alessandro, F., Frega, F., Francone, A., and Tomasicchio, G. R.: Improvement of a coastal vulnerability index and its application along the Calabria Coastline, Italy, Sci. Rep., 12, 21959, https://doi.org/10.1038/s41598-022-26374-w,
25 2022.

Paprotny, D., Terefenko, P., Giza, A., Czapliński, P., and Vousdoukas, M. I.: Future losses of ecosystem services due to coastal erosion in Europe, Sci. Total Environ., 760, 144310, https://doi.org/10.1016/j.scitotenv.2020.144310, 2021.

The Global Airport Database: http://www.partow.net/miscellaneous/airportdatabase/, last access: 10 November 2021.

Pekel, J.-F., Cottam, A., Gorelick, N., and Belward, A. S.: High-resolution mapping of global surface water and its long-term
30 changes, Nature, 540, 418–422, https://doi.org/10.1038/nature20584, 2016.

Pronk: DeltaDEM: A Global Coastal Digital Terrain Model., https://doi.org/10.4121/21997565, 2023.

Ranasinghe, R., Ruane, A. C., Vautard, R., Arnell, N., Coppola, E., Cruz, F. A., Dessai, S., Islam, A. S., Rahimi, M., Ruiz Carrascal, D., Sillmann, J., Sylla, M. B., Tebaldi, C., Wang, W., and Zaaboul, R.: Climate Change Information for Regional

Impact and for Risk Assessment, edited by: Masson-Delmotte, V., Zhai, P., Pirani, A., Connors, S. L., Péan, C., Berger, S., Caud, N., Chen, Y., Goldfarb, L., Gomis, M. I., Huang, M., Leitzell, K., Lonnoy, E., Matthews, J. B. R., Maycock, T. K., Waterfield, T., Yelekçi, O., Yu, R., and Zhou, B., Clim. Change 2021 Phys. Sci. Basis Contrib. Work. Group Sixth Assess. Rep. Intergov. Panel Clim. Change, 1767–1926, https://doi.org/10.1017/9781009157896.014, 2021.

5   Rocha, C., Antunes, C., and Catita, C.: Coastal indices to assess sea-level rise impacts - A brief review of the last decade, Ocean Coast. Manag., 237, 106536, https://doi.org/10.1016/j.ocecoaman.2023.106536, 2023.

Rosendahl Appelquist, L. and Halsnæs, K.: The Coastal Hazard Wheel system for coastal multi-hazard assessment & management in a changing climate, J. Coast. Conserv., 19, 157–179, https://doi.org/10.1007/s11852-015-0379-7, 2015.

Scussolini, P., Aerts, J. C. J. H., Jongman, B., Bouwer, L. M., Winsemius, H. C., de Moel, H., and Ward, P. J.: FLOPROS: an
10   evolving global database of flood protection standards, Nat. Hazards Earth Syst. Sci., 16, 1049–1061, https://doi.org/10.5194/nhess-16-1049-2016, 2016.

Tiggeloven, T., de Moel, H., Winsemius, H. C., Eilander, D., Erkens, G., Gebremedhin, E., Diaz Loaiza, A., Kuzma, S., Luo, T., Iceland, C., Bouwman, A., van Huijstee, J., Ligtvoet, W., and Ward, P. J.: Global-scale benefit–cost analysis of coastal flood adaptation to different flood risk drivers using structural measures, Nat. Hazards Earth Syst. Sci., 20, 1025–1044,
15   https://doi.org/10.5194/nhess-20-1025-2020, 2020.

Vafeidis, A. T., Nicholls, R. J., McFadden, L., Tol, R. S. J., Hinkel, J., Spencer, T., Grashoff, P. S., Boot, G., and Klein, R. J. T.: A New Global Coastal Database for Impact and Vulnerability Analysis to Sea-Level Rise, J. Coast. Res., 244, 917–924, https://doi.org/10.2112/06-0725.1, 2008.

Vos, K., Deng, W., Harley, M. D., Turner, I. L., and Splinter, K. D. M.: Beach-face slope dataset for Australia, Earth Syst.
20   Sci. Data, 14, 1345–1357, https://doi.org/10.5194/essd-14-1345-2022, 2022.

Vos, K., Harley, M. D., Turner, I. L., and Splinter, K. D.: Pacific shoreline erosion and accretion patterns controlled by El Niño/Southern Oscillation, Nat. Geosci., 16, 140–146, https://doi.org/10.1038/s41561-022-01117-8, 2023.

Vousdoukas, M. I., Mentaschi, L., Voukouvalas, E., Bianchi, A., Dottori, F., and Feyen, L.: Climatic and socioeconomic controls of future coastal flood risk in Europe, Nat. Clim. Change, 8, 776–780, https://doi.org/10.1038/s41558-018-0260-4,
25   2018.

Vousdoukas, M. I., Mentaschi, L., Hinkel, J., Ward, P. J., Mongelli, I., Ciscar, J.-C., and Feyen, L.: Economic motivation for raising coastal flood defenses in Europe, Nat. Commun., 11, 2119, https://doi.org/10.1038/s41467-020-15665-3, 2020a.

Vousdoukas, M. I., Ranasinghe, R., Mentaschi, L., Plomaritis, T. A., Athanasiou, P., Luijendijk, A., and Feyen, L.: Sandy coastlines under threat of erosion, Nat. Clim. Change, 10, 260–263, https://doi.org/10.1038/s41558-020-0697-0, 2020b.

30   Wolff, C., Vafeidis, A. T., Lincke, D., Marasmi, C., and Hinkel, J.: Effects of Scale and Input Data on Assessing the Future Impacts of Coastal Flooding: An Application of DIVA for the Emilia-Romagna Coast, Front. Mar. Sci., 3, https://doi.org/10.3389/fmars.2016.00041, 2016.

World Bank: GDP, PPP (constant 2017 international $, 2022.

Global Railways: https://geonode.wfp.org/layers/geonode%3Awld_trs_railways_wfp, last access: 10 November 2022.

Young, A. P. and Carilli, J. E.: Global distribution of coastal cliffs, Earth Surf. Process. Landf., 44, 1309–1316, https://doi.org/10.1002/esp.4574, 2019.

Zanaga, D., Van De Kerchove, R., De Keersmaecker, W., Souverijns, N., Brockmann, C., Quast, R., Wevers, J., Grosu, A., Paccini, A., Vergnaud, S., Cartus, O., Santoro, M., Fritz, S., Georgieva, I., Lesiv, M., Carter, S., Herold, M., Li, L., Tsendbazar, N.-E., Ramoino, F., and Arino, O.: ESA WorldCover 10 m 2020 v100, https://doi.org/10.5281/zenodo.5571936, 2021.

van Zelst, V. T. M., Dijkstra, J. T., van Wesenbeeck, B. K., Eilander, D., Morris, E. P., Winsemius, H. C., Ward, P. J., and de Vries, M. B.: Cutting the costs of coastal protection by integrating vegetation in flood defences, Nat. Commun., 12, 6533, https://doi.org/10.1038/s41467-021-26887-4, 2021.

Tables

Table 1: Summary of all the datasets used for the generation of the global coastal characteristics database.

Dataset name	Type	Description	Purpose	Reference
OSM coastline (zoom 8 level) 2016	Vector (lines)	Generalized coastline from Open Street Maps	Describe the global location of the shoreline and create the transects.	(Generalized coastlines, 2016)
CopernicusDEM (GLO-30)	Raster	Global topographic raster dataset at ~30 m resolution	Extract the subaerial part (topography) of the elevation profiles and the profile of the water mask used in GLO-30.	(Airbus Defence and Space GmbH, 2020)
DeltaDEM	Raster	Global coastal topographic raster dataset at ~30 m resolution	Extract the subaerial part (topography) of the elevation profiles.	(Pronk, 2023), unclipped version with values above 10 m +MSL
GEBCO 2023 Grid	Raster	Global bathymetric raster dataset at ~500 m resolution	Extract the submerged part (bathymetry) of the elevation profiles.	(GEBCO Bathymetric Compilation Group, 2023)
DTU10_MDT	Raster	Global Mean Dynamic Topography	Transform topographic elevation from the EGM2008 geoid reference to mean sea level (MSL) vertical reference.	(Knudsen and Andersen, 2013)
ESA World Cover (v100)	Raster	Global land cover class raster at ~10 m resolution	Classify coastal protection and extract the main land cover class for each transect.	(Zanaga et al., 2021)
JRC water occurrence	Raster	Global raster of water occurrence at ~ 30 m resolution	Get profile of water occurrence and extract transition zone width.	(Pekel et al., 2016)
Global distribution of sandy beaches	Vector (point)	Geolocation of sandy beaches worldwide	Identify the occurrence of sand at a transect.	(Luijendijk et al., 2018)
Global occurrence of saltmarshes and mangroves	Vector (point)	Geolocation of coastal segments with mangroves or saltmarshes	Identify the occurrence of vegetation at a transect.	(van Zelst et al., 2021)
ERA5	Raster (but points extracted for analysis)	Atmospheric, land and oceanic climate variables reanalysis	Extract the offshore significant wave height, peak period, mean wave direction, local temperature and precipitation indicators at each transect.	(Hersbach et al., 2020)

GTSM_v3.0	Vector (point)	Storm surge and tide reanalysis using a global hydrodynamic Delft3D Model	Extract tide, surge and total water level indicators at each transect.	(Muis et al., 2020)
WorldPop	Raster	Global population count per pixel at ~100 m resolution	Calculate the population indicators at each transect.	(Bondarenko et al., 2020)
World Bank GDP dataset	Tabular	GDP and GDP/capita for all countries	Characterize the GDP/capita per transect.	(World Bank, 2022)
Gridded global GDP	Raster (but points extracted for analysis)	GDP and GDP/capita for all countries	Characterize the GDP/capita per transect.	(Kummu et al., 2018)
gRoads_v1	Vector (lines)	Global Roads Inventory Network	Identify presence of roads at a transect.	(Meijer et al., 2018)
World Port Index	Vector (points)	Geolocation of major ports	Identifypresence of a port in the proximity of a transect.	(National Geospatial-Intelligence Agency, 2019)
Global Airport Database	Vector (points)	Geolocation of major airports	Identify presence of a port in the proximity of a transect.	(The Global Airport Database, 2021)
Global Railways	Vector (lines)	Global railway lines vector from the World Food Programme	Identify presence of railways per transect.	(Global Railways, 2022)

Table 2: Summary of all the geophysical parameters included in GCC.

Parameter	Label	Units	Description
Transect id	id	-	Id of the transect in the form of BOX_{box corners}_{transect number in box}
Longitude	lon	degrees	Longitude of the centroid of the transect
Latitude	lat	degrees	Latitude of the centroid of the transect
Transect angle	angle	Degrees N	Angle of transect (from land to sea direction)
Coastal Max (first peak)	z_peak_first_{x}	m above MSL	First elevation peak found landwards of the shoreline using x: deltadem or copdem
Coastal Max (max peak 1 km)	z_peak_max_1km_{x}	m above MSL	Maximum elevation peak found between the shoreline and 1 km landwards of the shoreline using x: deltadem or copdem
Cross-shore location of Coastal Max (first peak)	x_peak_first_{x}	m	Cross-shore location of Coastal Max (first peak), with the transect's centroid as reference, using x: deltadem or copdem
Cross-shore location of Coastal Max (max peak 1 km)	x_peak_max_1km_{x}	m	Cross-shore location of Coastal Max (max peak 1 km), with the transect's centroid as reference, using x: deltadem or copdem
Land cover class of Coastal Max (first peak)	lu_peak_first_{x}	-	Land cover class of Coastal Max (first peak) as extracted from ESA Worldcover_v100 (DOI: 10.5281/zenodo.5571936), using x: deltadem or copdem
Land cover class of Coastal Max (max peak 1 km)	lu_peak_max_1km_{x}	-	Land cover class of Coastal Max (max peak 1 km) as extracted from ESA Worldcover_v100 (DOI: 10.5281/zenodo.5571936), using x: deltadem or copdem
Mean hinterland elevation	he	m above MSL	Mean elevation of the hinterland, landwards of Coastal Max (first peak) and excluding water areas, using deltadem
Variance of hinterland elevation	ev	m^2	Variance of the elevation of the hinterland, landwards of Coastal Max (first peak) and excluding water areas, using deltadem
Depth of Closure	doc	m	Depth of closure found using Athanasiou et al. 2019 (https://doi.org/10.5194/essd-11-1515-2019). If distance of offshore location larger than 150 km a value of -10 m was assumed
Depth of Closure used	doc_used	m	Depth of closure used for slopes calculations in case the actual doc value was not available in the extracted profile
Cross-shore location of Depth of Closure	x_doc	m	Cross-shore location of Depth of Closure which was used in the profile, with the transect's centroid as reference

Cross-shore location of shoreline	x_shoreline	m	Cross-shore location of shoreline, with the transect's centroid as reference
Nearshore slope	ns	-	Nearshore slope calculated between the Depth of Closure and shoreline points
Backshore slope	bs_{x}	-	Backshore slope calculated between the shoreline and Coastal Max (first peak) points, using x: deltadem or copdem
Coastal slope	cs_{x}	-	Coastal slope calculated between the Depth of Closure and Coastal Max (first peak) points), using x: deltadem or copdem
Errors / Warnings	errors	-	0: No errors/warnings 1: Shoreline not found 2: Depth of Closure not available. Default -10 m used, 3: Depth of Closure is deeper than the deepest profile point (which is used for the calculation), 4: Coastal Max (first peak) could not be found
Width of transition zone	tr_zone_width	m	Width of transition zone defined as the two points around the shoreline with 5 and 95 % water occurrence as extracted from Pekel at al. 2016 (https://doi.org/10.1038/nature20584)
x land cover class occurrence	lu_{x}	%	Occurrence of land-cover class from the classes 'Trees', 'Shrubland', 'Grassland', 'Cropland', 'Built-up', 'Barren / sparse vegetation', 'Snow and ice', 'Open water', 'Herbaceous wetland', 'Mangroves', 'Moss and lichen' from the ESA Worldcover_v100 (DOI: 10.5281/zenodo.5571936). This is calculated in 500 m buffer zone around the landwards part of the transect
Main land cover class	class_most	-	Most encountered land cover class from ESA Worldcover_v100 (DOI: 10.5281/zenodo.5571936). This is calculated in 500 m buffer zone around the landwards part of the transect
Main land cover class excluding open-water	class_most_land	-	Most encountered land cover class from ESA Worldcover_v100 (DOI: 10.5281/zenodo.5571936) excluding the open-water class. This is calculated in 500 m buffer zone around the landwards part of the transect.
Sand occurrence	flag_sandy	-	Occurrence (1) or not (0) of sand in the proximity of the transect, based on Luijendijk et al. 2018 (DOI: 10.1038/s41598-018-24630-6)
Vegetation type	veg_type	-	Occurrence of mangrove or saltmarsh vegetation in the proximity of the transect based on van Zelst et al. 2022 (DOI: 10.1038/s41467-021-26887-4)
Mean Dynamic Topography	mdt	m	Difference between MSL and the geoid extracted at the centroid of the transect with bilinear interpolation from DTU10_MDT (Knudsen and Andersen 2013))

Table 3: Summary of all the hydrodynamic parameters included in GCC.

Parameter	Label	Units	Description
Hs 50th percentile	swh_p50	m	50th percentile of significant height of combined wind waves and swell (1979-2019) extracted from ERA5 (DOI: 10.1002/qj.3803)
Hs 95th percentile	swh_p95	m	95th percentile of significant height of combined wind waves and swell (1979-2019) extracted from ERA5 (DOI: 10.1002/qj.3803)
Tp 50th percentile	pp1d_p50	s	50th percentile of Peak wave period (1979-2019) extracted from ERA5 (DOI: 10.1002/qj.3803)
Tp 95th percentile	pp1d_p95	s	95th percentile of Peak wave period (1979-2019) extracted from ERA5 (DOI: 10.1002/qj.3803)
Average MWD of Hs ≥ Hs_p95	mwd_p95	degrees N	Average Mean Wave Direction (MWD) relative to true North, when Hs ≥ Hs_p95 (1979-2019) extracted from ERA5 (DOI: 10.1002/qj.3803)
Mean daily temperature 50th percentile	t2m_p50	degrees Celsius	50th percentile of mean daily temperature (1979-2019) extracted from ERA5 (DOI: 10.1002/qj.3803)
Mean daily temperature 95th percentile	t2m_p95	degrees Celsius	95th percentile of mean daily temperature (1979-2019) extracted from ERA5 (DOI: 10.1002/qj.3803)
Total daily precipitation 50th percentile	tp_p50	mm	50th percentile of total daily precipitation (1979-2019) extracted from ERA5 (DOI: 10.1002/qj.3803)
Total daily precipitation 95th percentile	tp_p95	mm	95th percentile of total daily precipitation (1979-2019) extracted from ERA5 (DOI: 10.1002/qj.3803)
Mean Higher High Water	mhhw	m above MSL	Mean Higher High Water (MHHW) (1985-2014) extracted from GTSMv3.0 (DOI: 10.3389/fmars.2020.00263)
Mean Lower Low Water	mllw	m above MSL	Mean Lower Low Water (MLLW) (1985-2014) extracted from GTSMv3.0 (DOI: 10.3389/fmars.2020.00263)
SSL 50th percentile	ssl_p50	m	50th percentile of storm surge level (SSL) (1985-2014) extracted from GTSMv3.0 (DOI: 10.3389/fmars.2020.00263)
SSL 95th percentile	ssl_p95	m	95th percentile of storm surge level (SSL) (1985-2014) extracted from GTSMv3.0 (DOI: 10.3389/fmars.2020.00263)
SSL (x years RP)	ssl_rp{x}_mean	m	Storm surge level (SSL) with return period of x: 1, 2, 5, 10, 25, 50, 100 years, from a GPD fit (1985-2014) extracted from GTSMv3.0 (DOI: 10.3389/fmars.2020.00263)
TWL (x years RP)	twl_rp{x}_mean	m above MSL	Total water level (TWL) with return period of x: 1, 2, 5, 10, 25, 50, 100 years, from a GPD fit (1985-2014) extracted from GTSMv3.0 (DOI: 10.3389/fmars.2020.00263)

Table 4: Summary of all the socioeconomic parameters included in GCC.

Parameter	Label	Units	Description
Country name	country	-	Country standard name that the transects belongs to derived from the WorldPop (DOI: 10.5258/SOTON/WP00685) dataset
Number of people	pop_all	People	Total number of people located in 500 buffer area. This is calculated in 500 m buffer zone around the landwards part of the transect using the WorldPop (DOI: 10.5258/SOTON/WP00685) dataset
Number of people below x elevation	pop_{x}_m	People	Total number of people located in 500 buffer area and below an elevation x: 1, 5, and 10 m. This is calculated in 500 m buffer zone around the landwards part of the transect using the WorldPop (DOI: 10.5258/SOTON/WP00685) dataset
Roads occurrence	roads	-	Intersection of transect with roads (1) or not (0) using the gROADSv1 (DOI: 10.1088/1748-9326/aabd42) dataset
Railways occurrence	railways	-	Intersection of transect with railways (1) or not (0) using the WFP Global Railways dataset (https://geonode.wfp.org/layers/geonode%3Awld_trs_railways_wfp).
Ports occurrence	ports	-	Port occurrence (1) or not (0) at a radius of 1 km around the transect using the WPI 2019 (https://msi.nga.mil/Publications/WPI) dataset.
Airports occurrence	airports	-	Airports occurrence (1) or not (0) at a radius of 1 km around the transect using the Global Airport Database (https://www.partow.net/miscellaneous/airportdatabase/).
GDP per capita PPP at 2015	gdp_ppp_usd2017_2015	USD (2017)	Gross Domestic Product (GDP) per capita based on purchasing power parity (PPP) at 2015, in USD 2017, extracted from the World Bank (https://data.worldbank.org/indicator/NY.GDP.MKTP.PP.KD) database based on the transect's country.
Gridded GDP per capita PPP at 2015	gdp_ppp_grid_2015	USD (2011)	Gridded Gross Domestic Product (GDP) per capita based on purchasing power parity (PPP) at 2015, in USD 2011, extracted from Kummu et al. 2015 (DOI: 10.1038/sdata.2018.4).

Figures
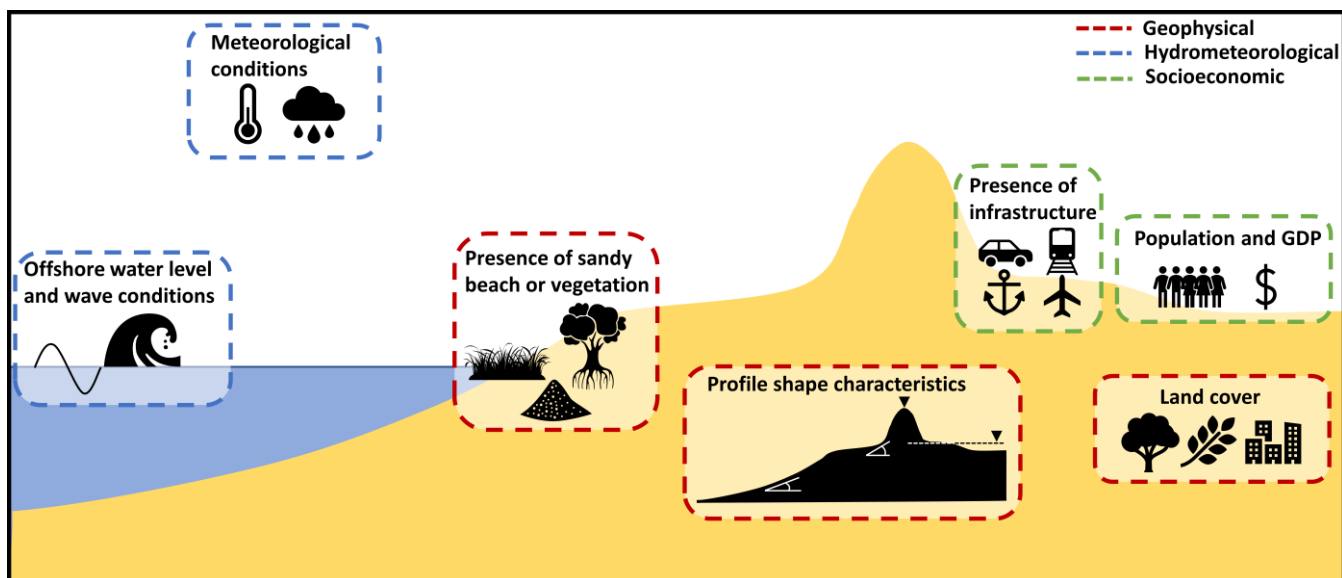
Figure 1: Overview of indicator groups extracted per transect globally. Indicators cover a wide range of coastal conditions, including the 1) geophysical (presence of sand or vegetation, profile shape characteristics and land cover), 2) hydrometeorological (offshore water level and wave conditions) and meteorological indicators and 3) socioeconomic environment (population, GDP and presence of critical infrastructure).
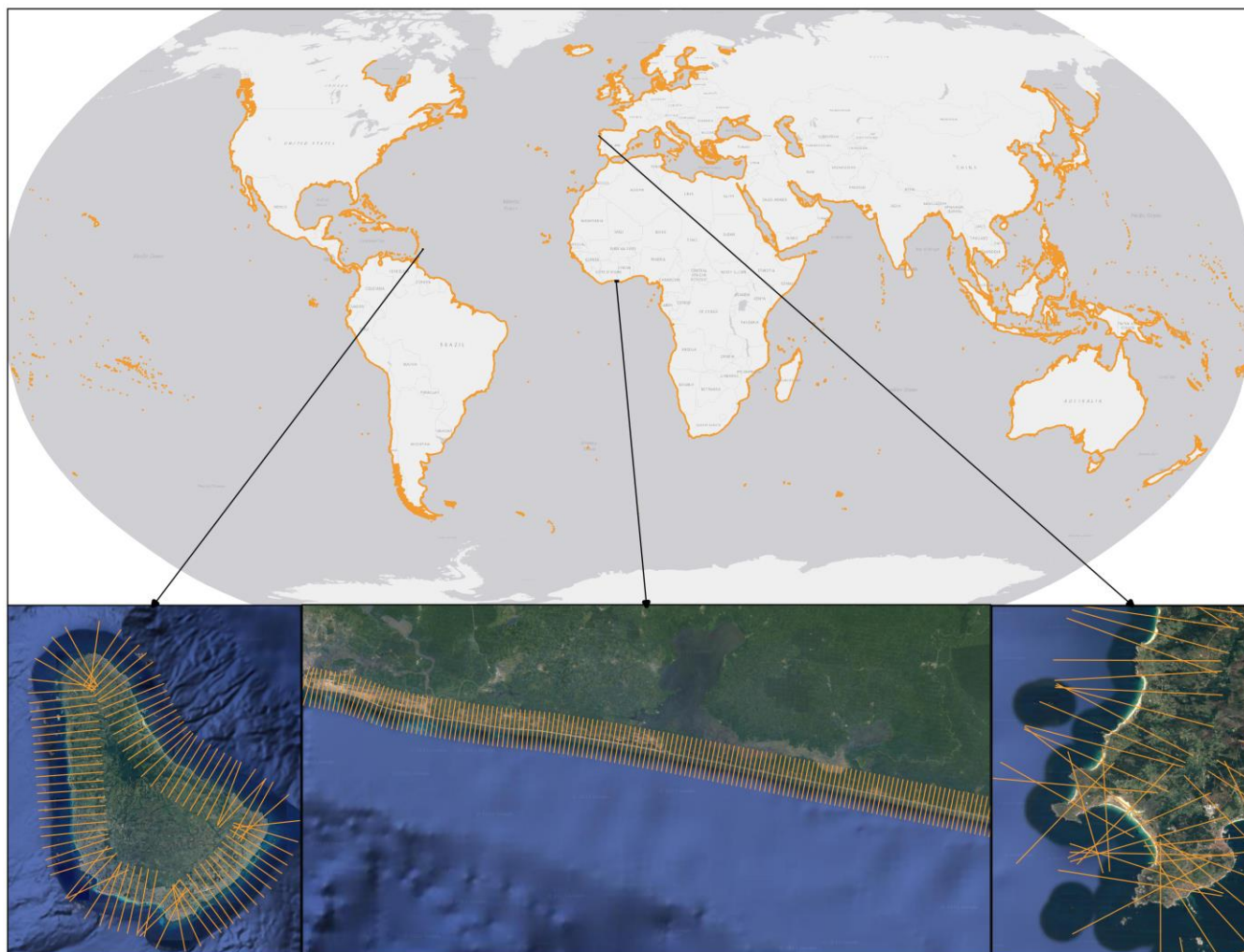
Figure 2: Top: Global coverage of the transect system. Bottom-left: Zoom in on Barbados. Bottom-centre: Zoom in on Ghana. Bottom-right: Zoom in on the west coast of Spain (Map data © Google Maps 2018).
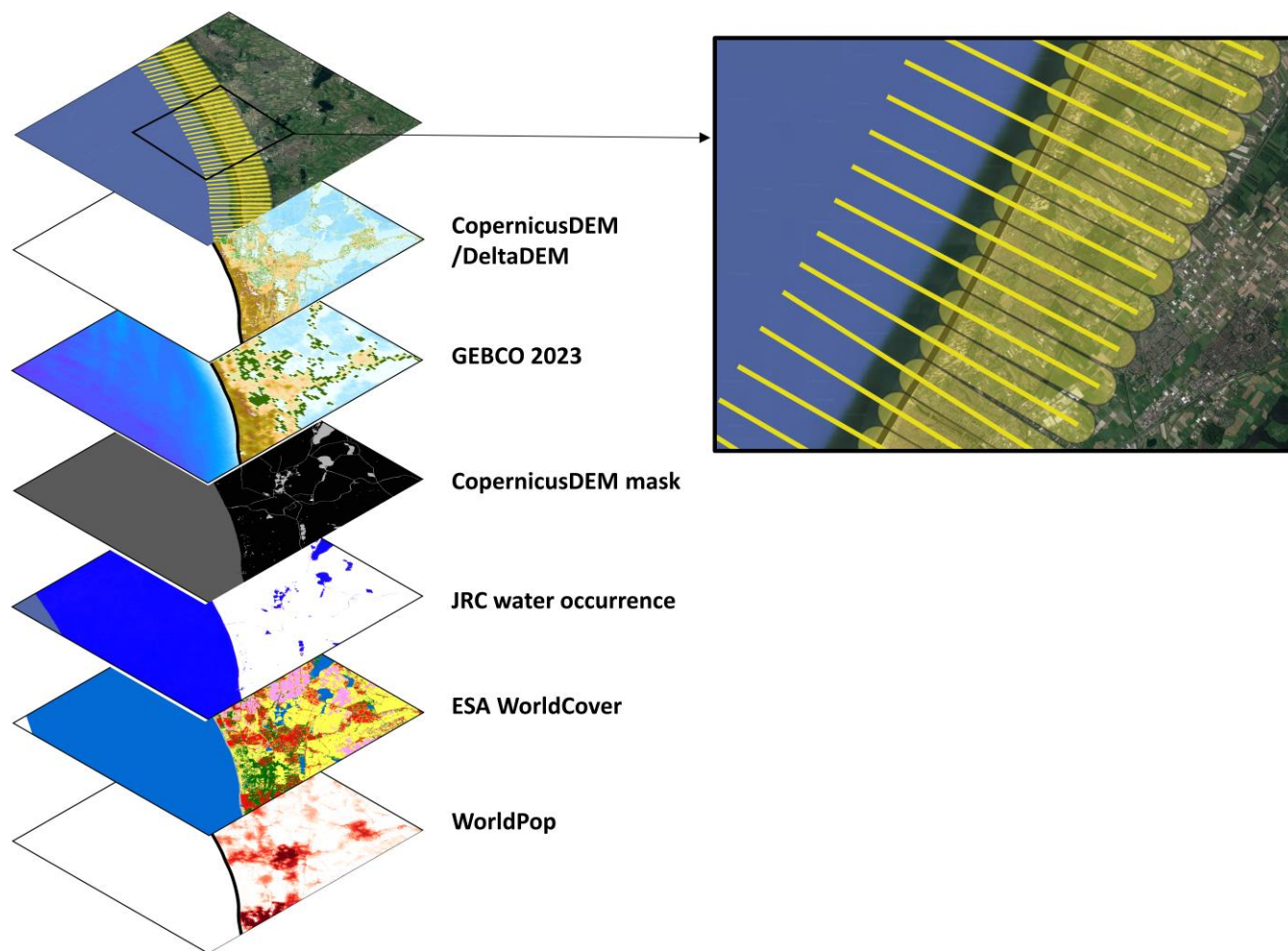
Figure 3: Raster datasets used for extracting transect information. The zoom-in shows the transects (yellow lines) along which the profiles were extracted, and the buffer zones (yellow areas) in which zonal statistics were performed (Map data © Google Maps 2018).
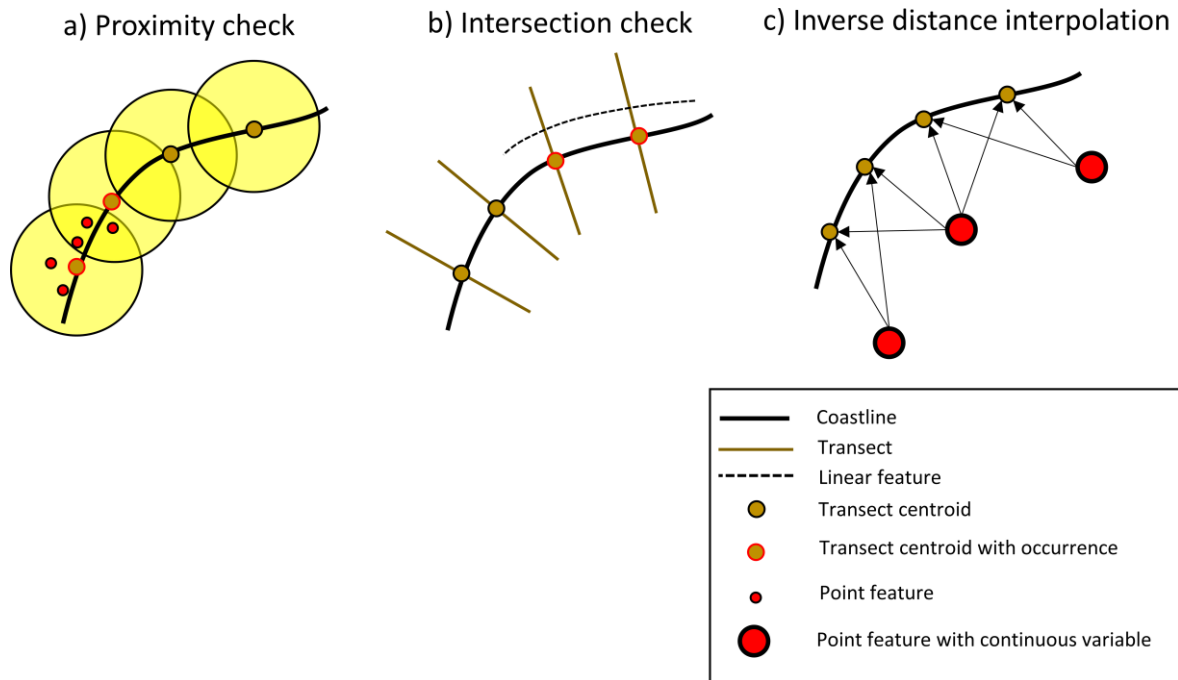
Figure 4: Schematic representation of the three methods followed to sample vector data to the transects for an indicative example coastline with four transects. a) Proximity check identifies if there are point features in a buffer zone around the centroid of a transect, b) Intersection check, identifies if the transect is intersecting a line feature and c) Inverse distance interpolation, uses the two closest points to get a distance weighted estimate at the transect.
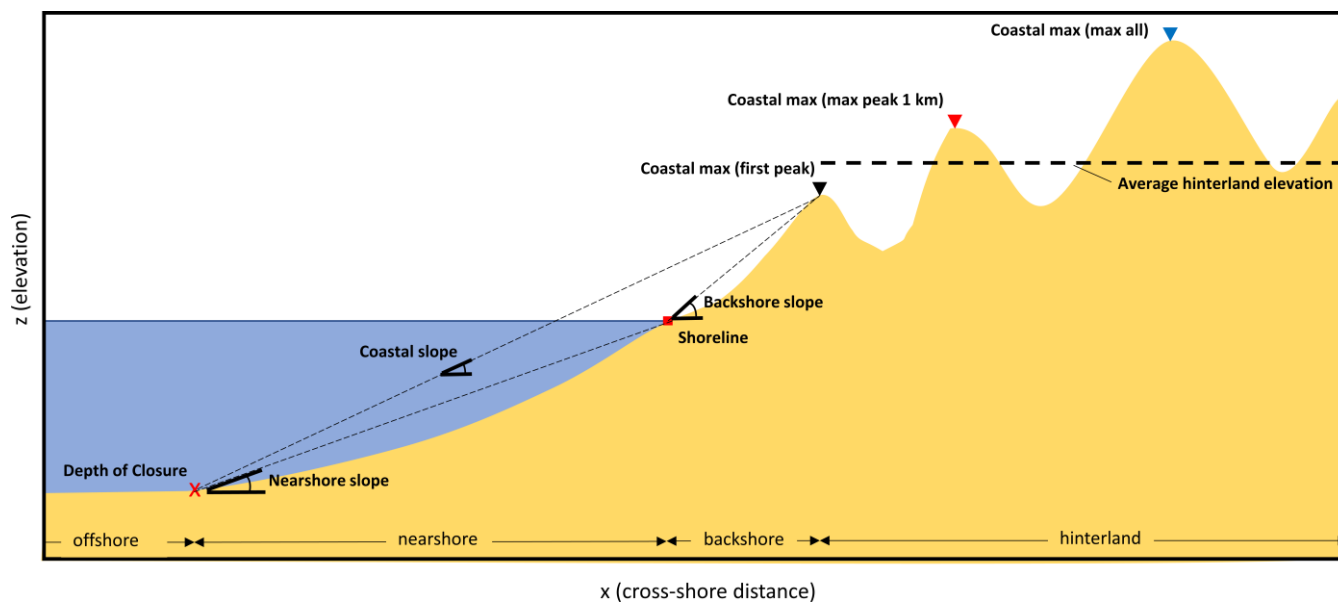
Figure 5: Schematic representation of the geophysical characteristics that are extracted per elevation profile
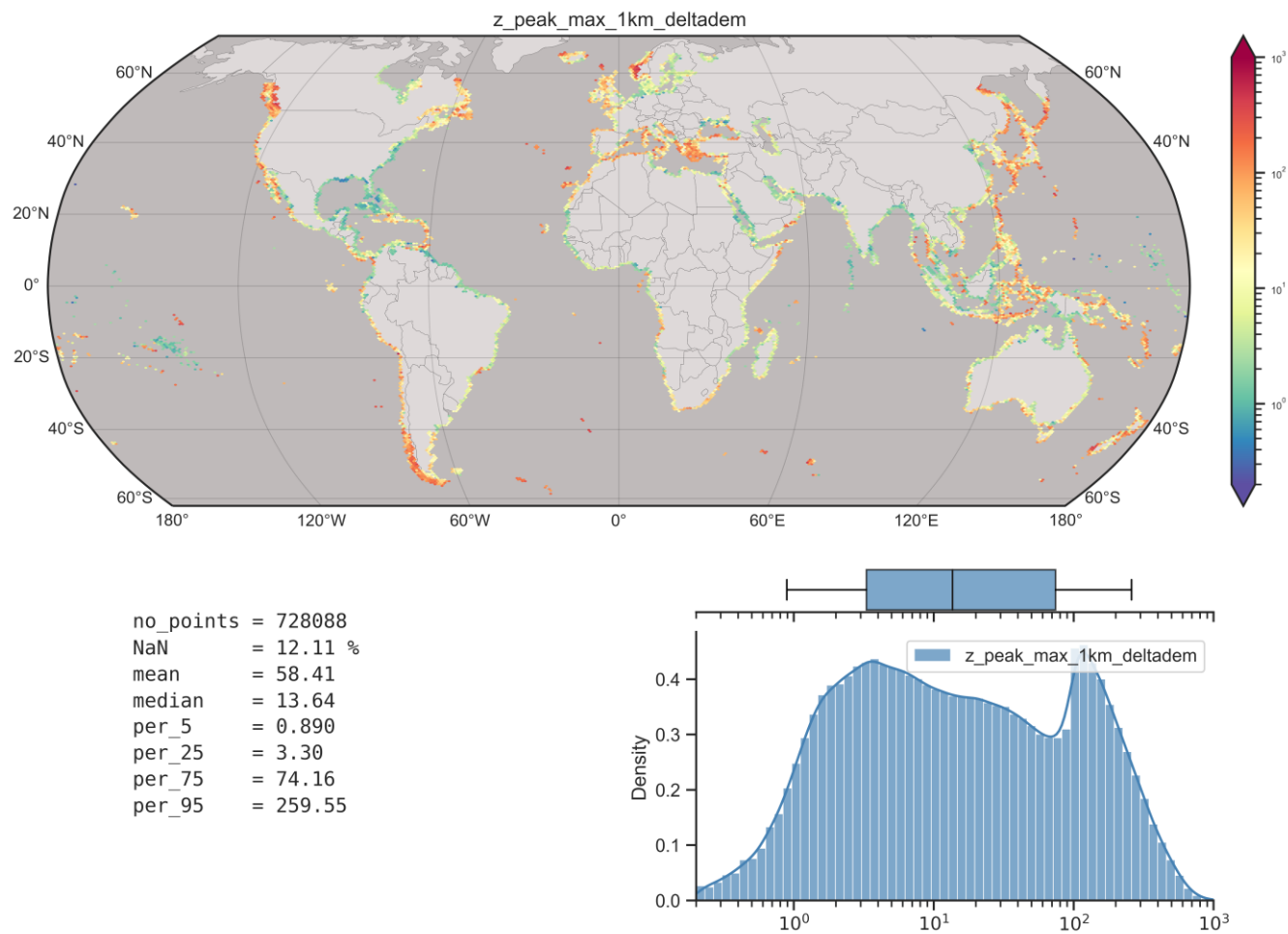
Figure 6: Global map and statistics of the Coastal max (max peak 1km) using deltadem. Top: Global map showing the median values in hexagons with a size of ~1 degree. The color bar is given in a logarithmic scale. Bottom right: Histogram and boxplot (with the lines showing the 5th and 95 percentiles, the box the 25th and 75th percentiles, and the vertical line the median) of Coastal max (max peak 1km) at the transect level. The x is plotted in logarithmic scale. Bottom left: various global statistics.
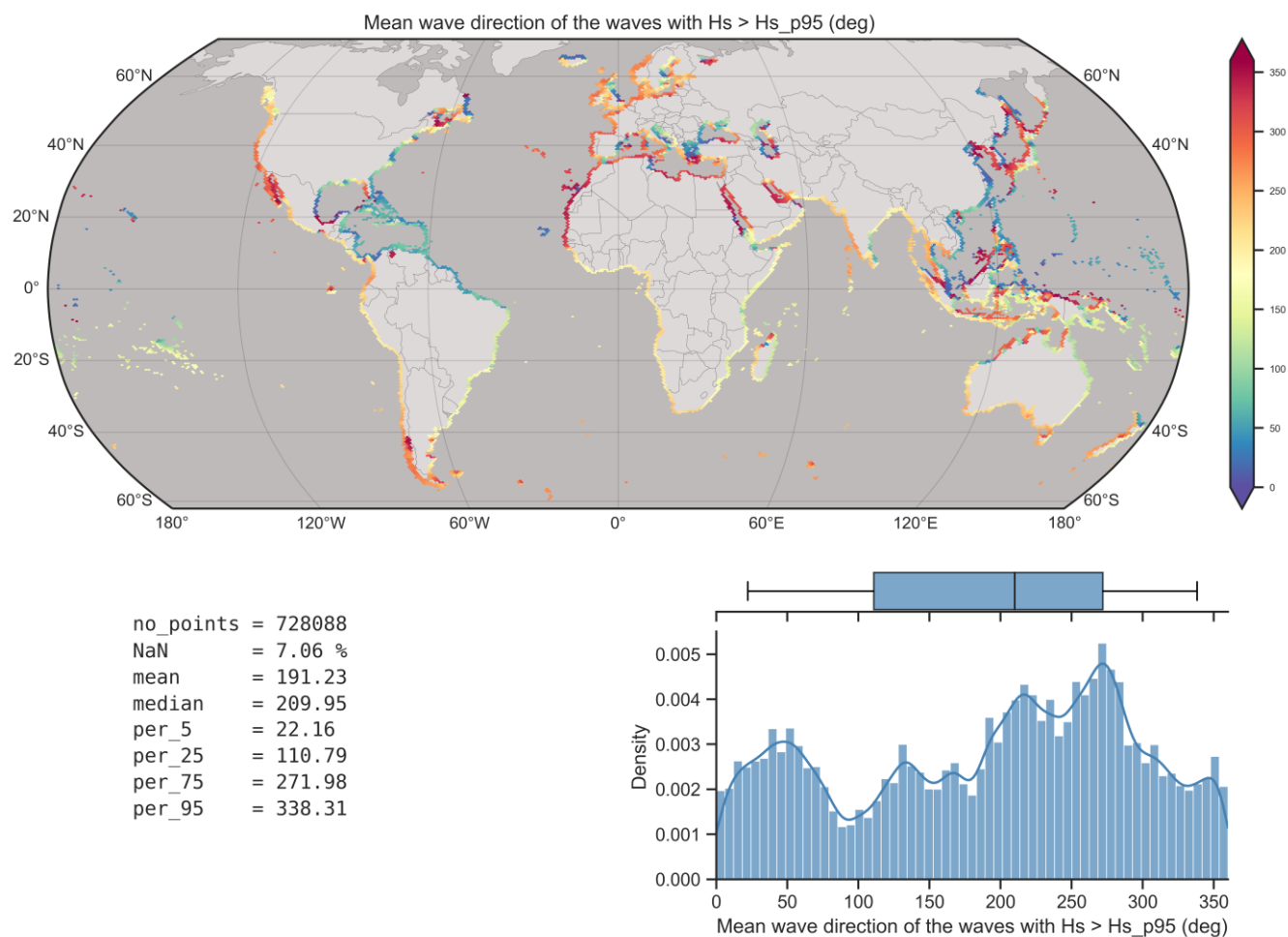
Figure 7: Global map and statistics of Average Mean Wave Direction (MWD) relative to true North, when Hs ≥ Hs_p95 (1979-2019). Top: Global map showing the median values in hexagons with a size of ~1 degree. Bottom right: Histogram and boxplot (with the lines showing the 5th and 95 percentiles, the box the 25th and 75th percentiles, and the vertical line the median) of Average Mean Wave Direction (MWD) at the transect level. Bottom left: various global statistics.
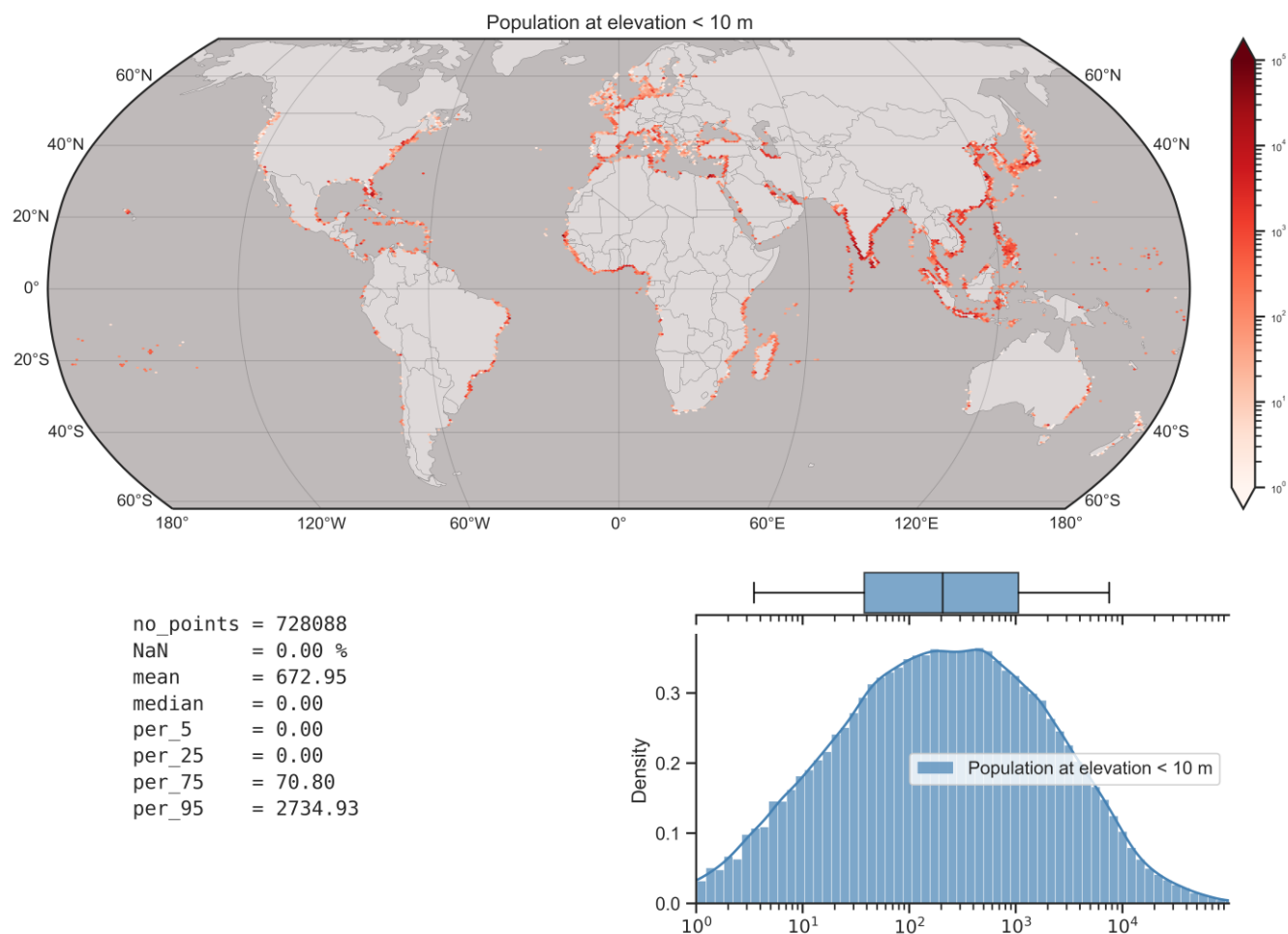
Figure 8: Global map and statistics of population at elevation < 10 m. Top: Global map showing the median values in hexagons with a size of ~1 degree. Hexagons with no population are not plotted. Colorbar is given in a logarithmic scale. Bottom right: Histogram and boxplot (with the lines showing the 5th and 95 percentiles, the box the 25th and 75th percentiles, and the vertical line the median) describing the transects with at least one person. The x axis is plotted in logarithmic scale. Bottom left: various global statistics (including transects with 0 population at elevation < 10 m).
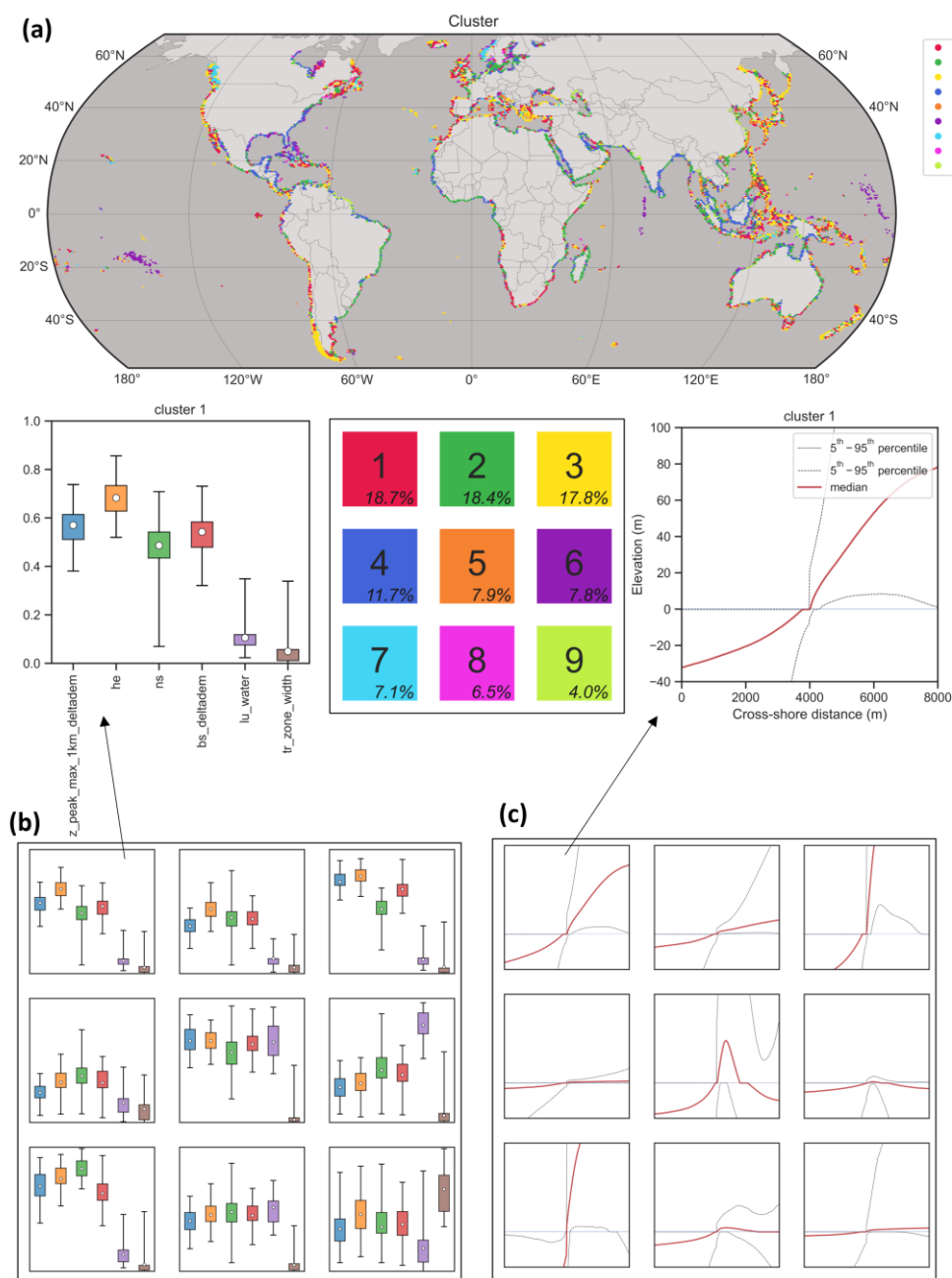
Figure 9: Geophysical clustering of the global transects with K-means into nine clusters using the *coastal Max (max peak 1 km)*, *mean hinterland elevation*, *nearshore slope*, *backshore slope*, *open-water land cover class occurrence and the transition zone width* as clustering parameters. (a) Global map showing the most frequent cluster in hexagons with a size of ~1 degree. The cluster number, frequency of appearance and color are shown in the grid in the middle, which is the same order as the grid at panels b and c. Cluster numbers are ordered by frequency of appearance. (b) Boxplots of intra-cluster scaled parameters variability. Boxes define the 25–75% percentile, lines the 5–95% percentile and circles indicate the centroid of each cluster. (c) Cluster elevation profile variability.